JOURNAL OF OPTOELECTRONICS AND ADVANCED MATERIALS Vol. 8, No. 6, December 2006, p. 2044 - 2050

Towards an atomistic understanding of phase change materials

C. STEIMER*, W. WELNIC, J. KALB, MATTHIAS WUTTIG
I. Institute of Physics (IA), RWTH-Aachen University, D52056 Aachen, Germany

Despite their widespread commercial applications, phase change alloy optimization still heavily relies on trial and error. While the crystalline structures are accessible by diffraction, the structures of the amorphous phases are still fairly unknown and thus hamper an atomistic understanding of the speed and pronounced property contrast on crystallization. This contribution gives an overview on the current understanding of the influence of stoichiometry on both phases. The recent renaissance of phase change materials raised by non-volatile electronic memory applications triggered remarkable insight in some amorphous structures, leading to an atomistic understanding of the phase change process that may be turned into design rules for future materials.

(Received November 3, 2006; accepted November 2, 2006)

Keywords: $AgInTe_2$, $AgSbTe_2$, Phase change materials, Non-volatile electronic memory

1 Introduction

Phase-change recording employs ns-duration laser- or electrical current-pulses of high intensity to melt a sub-micron sized spot of crystalline material. By subsequent quenching the spot reaches its amorphous state. A second pulse of lower intensity but longer duration heats also the surrounding material to yield lower temperature gradients and cooling rates to erase the bit by re-crystallization. The difference in the optical and electrical properties of both states allows reading out the bit by a third pulse to low in intensity to change the material [1]. Fig. 1 sketches the operation-principle.

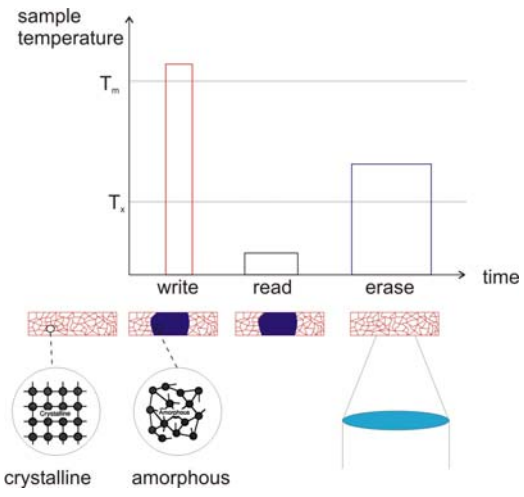

Fig. 1. Operation Principle of PC-storage.

The key parameters are a sufficient electrical and optical contrast between the amorphous and the crystalline state to ensure easy reading as well as the time required for re-crystallization that limits the data-transfer-rate. While large structural differences of the amorphous and the crystalline phase give rise to large contrast, they might slow down re-crystallization. Until now the search for suitable materials has been entirely empirically. Only recently, atomistic models for the amorphous phase of two prototype phase change materials have been put forward. They will help to establish an atomistic understanding of the influence of stoichiometry on both crystalline and amorphous phases, which can then be turned into design rules for novel materials.

In the following, we discuss how stoichiometry influences the structure of the crystalline phase before turning to the amorphous short-range order. Then kinetic aspects will be considered before we come up with a summary of our current understanding and future challenges.

2. Stoichiometry and crystalline structures

Phase change materials can be divided into a Sb-rich and Te-rich class. They are mainly based on Sb_2Te or Sb_2Te_3-GeTe [2,3,4] and re-crystallize by fast growth or fast nucleation, respectively. The most prominent example of the Sb-rich materials is AgIn-doped Sb_2Te. Two of the phases formed upon annealing of AgIn doped Sb_2Te are $AgInTe_2$ and $AgSbTe_2$, which were chosen as model-systems for stoichiometry induced structural transitions [5]. The amorphous samples were prepared by physical vapor deposition on glass-substrates.

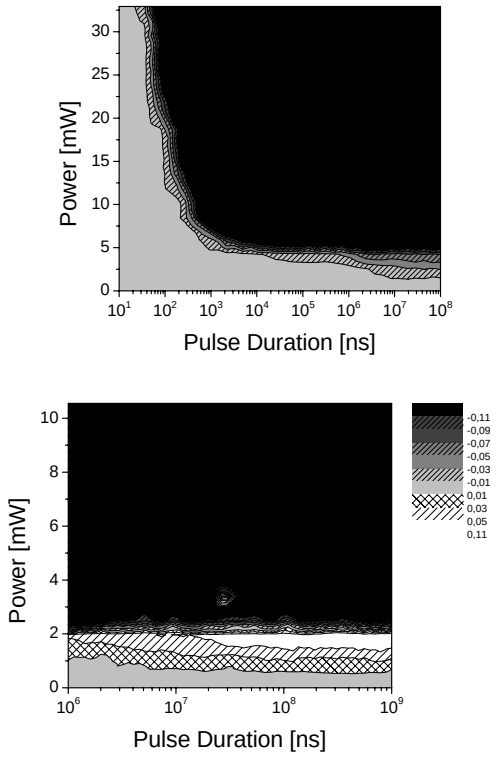

Fig. 2. Power-Time-Effect diagrams for $AgInTe_2$ and $AgSbTe_2$. The grayscale coded in- or decreases in reflectivity are attributed to crystallization or ablation, respectively [5].

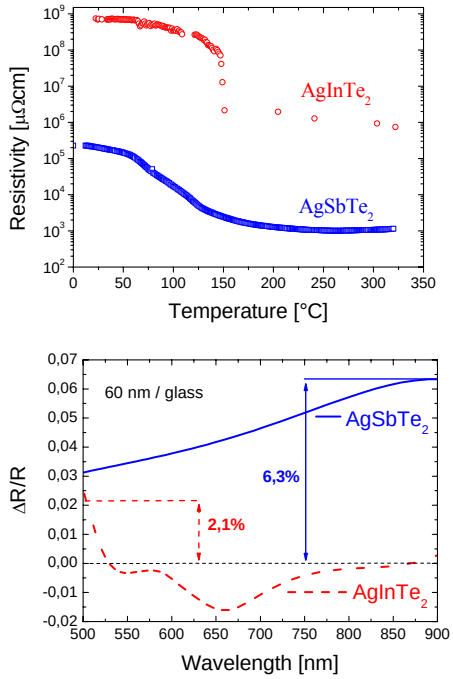

Fig. 3. Top: Sheet resistance of a 60 nm film on glass measured on annealing. Bottom: Optical contrast between amorphous and crystalline phase, calculated from ellipsometric measurements [5].

The reflectivity of each amorphous spot is measured before exposing them to crystallization pulses of defined intensity and duration. Then the reflectivity is determined again to obtain the effect of the crystallization pulse. Both measurements are performed with the same laser-diode and optics at 830 nm. This procedure was repeated for a 2-dimensional array of spots, where each point corresponds to a laser pulse with a different intensity or duration. The results are shown in figure 2: For low intensities and long pulse durations $AgSbTe_2$ shows an increase in reflectivity due to crystallization. For $AgInTe_2$ however, no evidence for crystallization is observed, i.e. no region with a positive reflectivity change is found: Despite their chemical similarity these model alloys show that not all Te-alloys exhibit an optical contrast sufficient for successful applications as phase change materials.

To understand that constant reflectivity of $AgInTe_2$, the sheet-resistance of as deposited samples was monitored during annealing in an inert atmosphere. Figure 3 shows the drop of resistivity beyond 100° C together with the optical contrast, calculated from the optical constants determined before and after annealing.

To relate the different optical contrasts with structure, XRD measurements were recorded for the annealed samples. They confirm crystallization in a chalcopyrite structure for $AgInTe_2$. $AgSbTe_2$ crystallizes in a rocksalt structure, where the Te-atoms occupy one of the sub-lattices while the remaining places are randomly occupied by Ag and Sb. The formation of a chalcopyrite structure up to average valence electron number N_{sp} of four and of octahedral arrangements like the rocksalt structure beyond that value can be understood by Density Functional Theory (DFT): For a preset structure DFT varies the electron density to minimize the ground state energy. We performed this calculations for a variety of $ABTe_2$-alloys with A = Cd, In, Sn, Sb; B = Ga, Ge, As, Sb [6]. For each alloy, the energies of the rocksalt and chalcopyrite structure were calculated and the lattice constant varied to obtain the optimum energy for each configuration. Fig. 4 shows the energy difference between these optima for a rocksalt -and a chalcopyrite structure. The different alloys indicate that this structural transition is a general rule for chalcogenides and not a peculiarity of $AgInTe_2$ and $AgSbTe_2$.

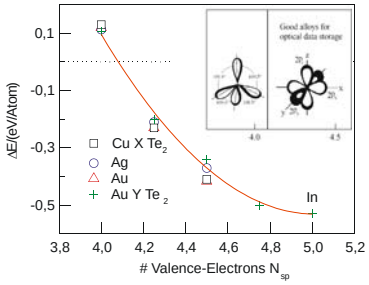

Fig. 4 Energy difference between rocksalt - and chalcopyrite structure, calculated by DFT for different model-alloys with varying number of valence electrons but constant ratio of constituents. X = Cd, In, Sn, Sb; Y = Ga, Ge, As, Sb; see [6] for details.

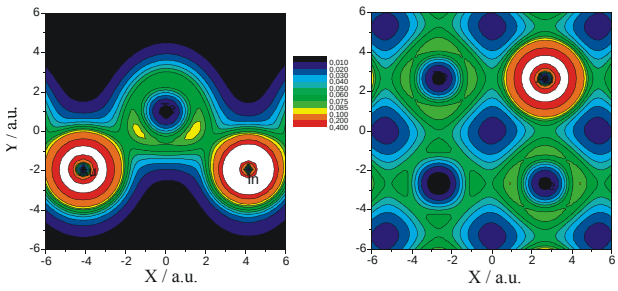

Fig. 5. Calculated electron-densities in arbitrary units for the (100)- and (111)-plane of $AuInTe_2$ (left) and $AuSbTe_2$ (right) with average valence electron numbers of 4.0 and 4.5 [6].

Choosing a chalcopyrite and a rocksalt structure for $AuInTe_2$ (N_{sp} =4.0) and $AuSbTe_2$ (N_{sp} =4.5) gives the electron density plots in Fg. 5, that explains the formation of chalcopyrite and rocksalt structures in a molecular orbital picture. Up to $N_{sp} = 4$, the valence electrons can be hosted in bonding sp^3 -orbitals that induce tetrahedral coordination. Beyond that value, occupation of orthogonal p-orbitals is preferred and thus octahedral coordination as found in simple cubic or rocksalt structures is facilitated. This trend is also reflected in a collection of experimental structural data of Luo [6] and earlier results on the structure of ABX_2-alloys (A=Cu,Ag; B=Ga,In,Tl/Sb,Bi/Fe, X=Se,Te) by Zhuze et al. [7].

Interestingly the materials with tetrahedral arrangements tend to show optical contrast that is insufficient for optical storage as opposed to the materials with octahedral coordinations. This behavior has been explained by the lower density contrast on amorphization of the tetrahedral structures. However this phenomenological description represents the structural change by the change of density alone and consequently reduces the wavelength-dependent contrast to a single number. To gain an atomistic understanding of phase change switching that correctly reproduces the energy-dependence of the contrast and can be reversed into design rules for improved materials, the amorphous structure has to be understood. In the next chapter we will come up with a model for the amorphous short-range order for materials with compositions along the GeTe-Sb_2Te_3 pseudo-binary line.

3. Amorphous short-range order and contrast

$Ge_2Sb_2Te_5$ is not just the most prominent example from that pseudo-binary line but most likely the most frequently investigated phase change material at all. Fig. 6, that compares its optical contrast between the amorphous and crystalline phase with GaAs as a prototype for covalently bonded alloys, is a good starting point to summarize the peculiar optical behavior of phase change materials: For conventional materials like GaAs, the dielectric function of the amorphous phase follows the crystalline one closely, except for a damping of the sharper features that are smeared-out to some extent in the amorphous state. However the relative variations never exceed about 25%.

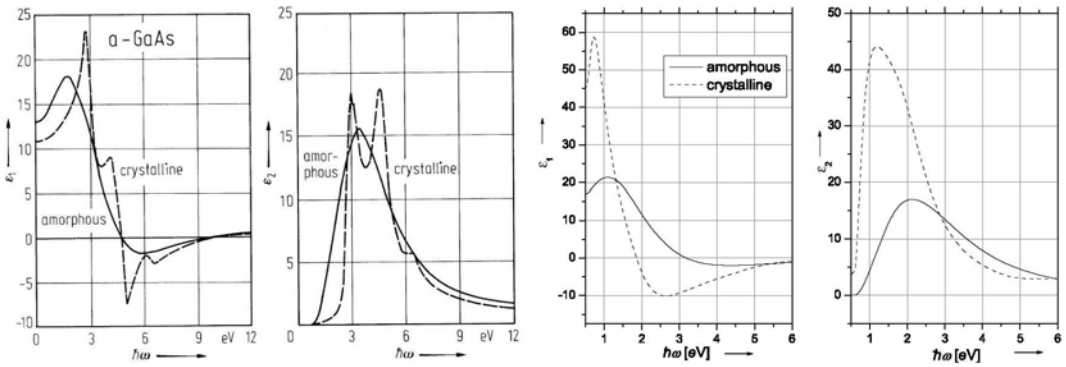

Fig. 6. Real and imaginary part of the dielectric function as a function of photon energy for GaAs from Landolt Börnstein and $Ge_2Sb_2Te_5$ [8] (right) in the crystalline and amorphous phase, respectively. To compare the difference for both states note the different scales.

This is by no means true for phase change alloys like $Ge_2Sb_2Te_5$, where differences as large as 150% are observed. This enormous optical difference can only be explained, if large structural changes appearing on short length-scales, that determine the optical and electronic properties, are assumed. Thus Kolobov [9] investigated the short-range order of crystalline and amorphous $Ge_2Sb_2Te_5$ by Extended X-ray Absorption Fine Structure (EXAFS).

EXAFS determines the short-range order in the vicinity of an element, selected with resonant X-rays, by electron diffraction at the surrounding shells. The Fourier-transformed EXAFS-signal yields a correlation-function, which is displayed in Fig. 7 for GaAs and $Ge_2Sb_2Te_5$ for the amorphous and crystalline state, respectively.

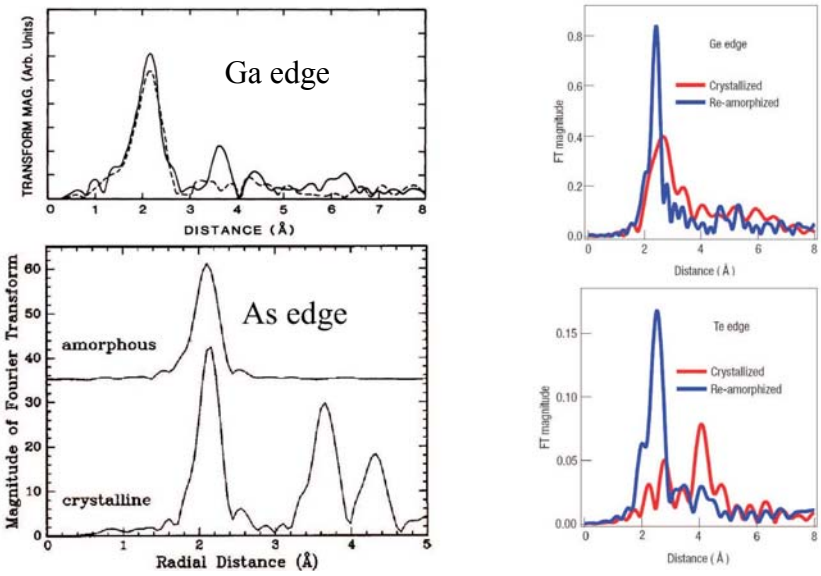

Fig. 7. Compilations of Fourier-transformed EXAFS-signals for the Ga-and As-edge of GaAs (left) [10,11] and the Ge-and Te-edge of $Ge_2Sb_2Te_5$ (right) [9] in the crystalline and amorphous phase from Rigday, Bouldin, Kolobov and their respective coworkers.

The short range order of the amorphous phase of GaAs differs from the crystalline counterpart only by the absence of higher order maxima and has a broader flattened appearance, due to the loss of long range order, both in the vicinity of the Ga and the As atoms. Again the situation is completely different for $Ge_2Sb_2Te_5$, where the correlation functions for all elements (Sb not shown here) differ substantially. This major change in near range order explains the large electronic and optical contrast of the dielectric functions visible in figure 6. Kolobov [9] related that contrast to a transition to a tetrahedral coordination of the Ge-atoms on amorphization by a shifting them towards vacancies in the GeSb-sub-lattice of the NaCl-structure of $Ge_2Sb_2Te_5$. Starting out from the idea of tetrahedral coordination of the Ge-atoms in the amorphous phase, we have looked for structures that could maintain an octahedral coordination for the Sb- and Te- atoms, but allow for tetrahedral places for the Ge-atoms. The spinel structure fulfills all requirements. It was thus chosen to model the short-range order of the amorphous phase for our DFT-calculations [12]. This approach introduces a long range order not present in the amorphous phase that could only be avoided by repeating the unit cell with additional variations to introduce a loss of long-range order. However as short-range order is responsible for the electronic and optical properties we are interested in, the effect of an artificial long-range order is acceptable to save computational time. For the same reason $Ge_1Sb_2Te_4$ and a cell of 64 sites were chosen. We calculated the ground state energies for the rocksalt and chalcopyrite structures established for the materials by XRD and compared them to the spinel-like order assumed for the amorphous phase. In all cases we varied the lattice constant (abscissa in Fig. 8) and allowed the atoms to relax from their ideal positions to sample different possible configurations. Fig. 8 compares the ground state energies per atom as a function of the lattice constant for the ideal and the relaxed rocksalt and spinel structure with the chalcopyrite-order, that is far off in energy. As relaxation did not show a visible effect on the chalcopyrite-energies, they are omitted in Fig. 8.

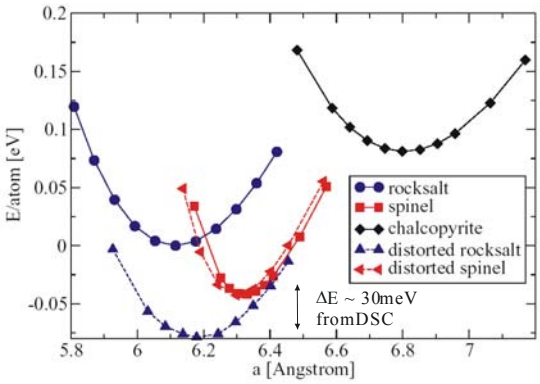

Fig. 8. Ground-state energy vs. lattice constant for the ideal and relaxed rocksalt -, spinel -and chalcopyrite structure. The energy difference and lattice expansion between the lowest energy (distorted rocksalt) and the second best structure, the spinel phase are in good agreement with experimental values for the difference between the crystalline and amorphous phase [12].

The relaxed spinel-structure has a minimum at a lattice constant of about 6.3 Å. The energy of that minimum is only 30 meV/atom higher than the overall minimum of the relaxed rocksalt structure. This difference in energy is well in line with current differential scanning calorimetry results [13]. The larger lattice constant also explains the large expansion of phase change materials with rocksalt structure on amorphization of about 5% as compared to 2% observed for the chalcopyrite alloys. Interestingly, although the Ge-atoms shift in space, the effect of the re-arrangements becomes visible most clearly on the Te-atoms, that are next to the Ge-sites. This change can be seen in figure 9, which gives the difference in the density of states between the relaxed rocksalt and spinel-structure. The increase of the overall density of states in Fig. 9a) just below the Fermi-level between 0 and –5 eV is indicative for a semiconductor-metal transition and a large optical contrast on crystallization. Note however, that the calculations tend to underestimate the band-gap. The plots separated for the elements and s- and p-bands 9b)-d) show, that these changes are related mostly to the p-bands of Te, while the Ge-contribution changes mainly in the s-band. The behavior of Sb is in between these two limiting cases. Overall the Te-p-bands deliver the main contribution to the changes on crystallization, that is easily identified in overall density of states 9a).

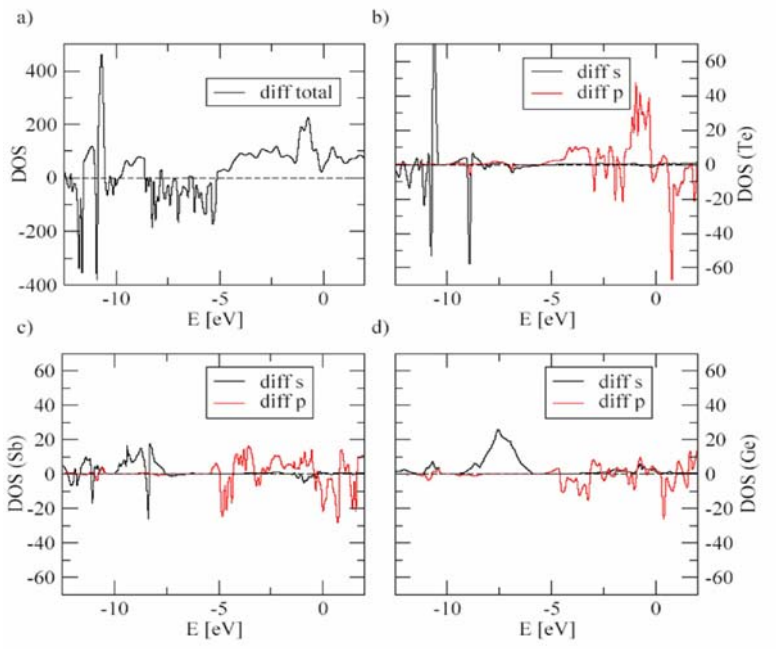

Fig. 9. Difference of the density of states between the relaxed rocksalt -and spinel structures for all atoms and for the s-and p-bands for each element [12].

Thus in conclusion our DFT-results are well in line with Kolobovs EXAFS-data and explain both the large density change and optical contrast.

Kinetics

As discussed in the introduction, another puzzle of this material class is its fast re-crystallization that needs to be combined with a long time stability of amorphous bits against crystallization for archival lifetime. The key parameter to reconcile these apparent contradictions is the temperature dependence of the mobility or the viscosity that varies by several orders of magnitude between room temperature and the glass and melting-transition where crystallization proceeds. Crystallization is a two-step process that involves the formation of crystalline nuclei and their subsequent growth. At temperatures below the glass transition temperature T_g, the driving force for the formation of crystalline nuclei is high, but the mobility of the atoms needed for their formation is low. The nucleation thus peaks at temperatures above T_g, which is about half of the melting temperature T_m for the alloys discussed here. At temperatures slightly below T_m the driving force for nucleation is small, but the high mobility induces a maximum of the growth rate. As a consequence, crystallization is fastest in an intermediate temperature range. Although both processes are well established since the thirties of the last centuries an atomistic understanding has been hampered by the experimental challenge to combine a high spatial with a high time resolution. Atomic Force Microscopy offers high spatial resolution at low temperatures, when kinetics are slowed down. Due to the higher density crystalline parts appear as dark impressions in amorphous films and a direct observation of nucleation

and growth with time and temperature as shown in figure 10 is possible.

AgIn doped Sb_2Te

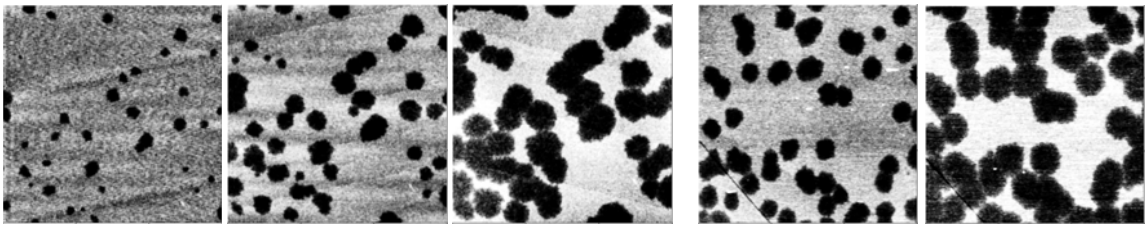

a) 160°C, 5 min b) 7 min c) 9 min d) 185°C, 6 sec e) 8 sec;

$Ge_4Sb_1Te_5$

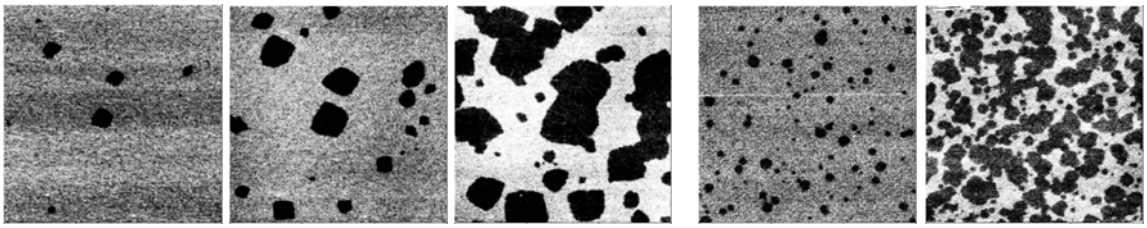

f) 140°C, 225 min g) 375 min h) 600 min i) 180°C, 11 sec j) 19 sec.

Fig. 10. AFM-pictures snapshots of the same 3×3 µm area (a-c, d-e, f-h, I-j) of an $AgInSb_2Te$ (a-e) and a $Ge_4Sb_1Te_5$ (f-j) film for 2 different temperatures each [3].

Comparing different temperatures shows an increase in growth velocity with temperature. There is no increase in crystallite number for AgIn-doped Sb_2Te neither in time nor in temperature. In $Ge_4Sb_1Te_5$ however, new nuclei are generated at all stages of the experiment and the nucleation rate increases with temperature. From the Arrhenius-plots of the growth velocity in Fig. 11, the activation barriers for growth can be determined. The similarity of the growth velocities and the activation barriers and the evolution of the number of nuclei show, that AgIn-doped Sb_2Te, that is usually referred to as a fast growth material, would be better described as a slow nucleation material [3].

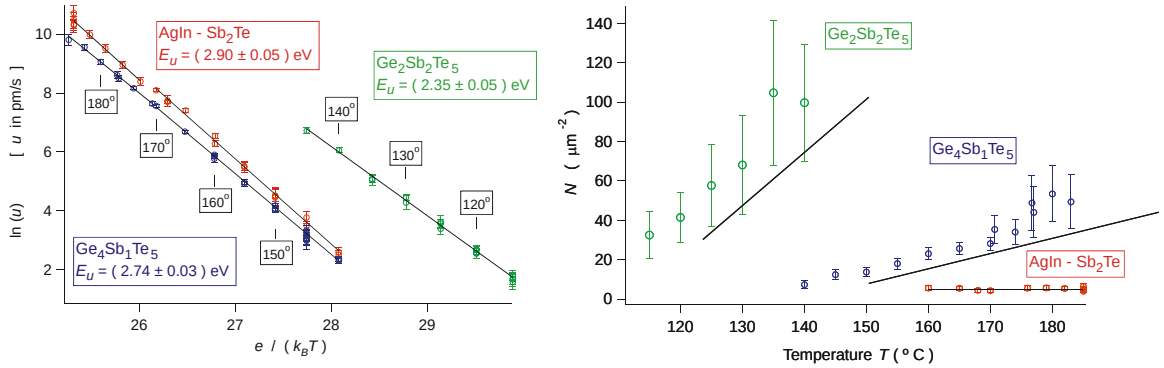

Fig. 11. Growth-velocity (left) and density of crystals from AFM-measurements for nucleation - and growth-dominated materials. While the activation energy for growth in the Arrhenius-plot on the left is similar, the crystal density shows a completely different behavior [3].

To understand the origin of this slow nucleation we have performed under-cooling experiments on phase change alloys, approaching crystallization from the high temperature regime [4]. With the other parameters known, a minimum value for the interfacial energy between the crystalline nucleus and the liquid matrix can be determined from the maximum under-cooling observed in a calorimeter. To prevent crystallization from the solid walls of a crucible, the samples were surrounded by a B_2O_3-flux that does not show any phase transitions in the

temperature range from 440 to 720 °C used in our Differential Scanning Calorimetry experiments (DSC) and provides a liquid sample container. Additionally B_2O_3 serves as a solvent for possible impurities as the samples were fluxed beyond their melting point for purification before the actual under-cooling experiments. The maximum under-cooling was determined from the inset of the exothermic heat of crystallization.

Table 2 gives the results obtained from these under-cooling experiments (see [4] for details). The key parameter for the nucleation rate is the product $\alpha^3 \beta$ with α the interfacial energy in units of the enthalpy of fusion and β is the entropy of fusion (all energies per atom). As the nucleation rate depends on the third power of the interfacial energy nucleation is mostly governed by α. Although the values for AgIn doped Sb_2Te and $Ge_4Sb_1Te_5$ are to close to be distinguished without doubt, there is a clear trend towards reduced values of $\alpha^3 \beta$ for nucleation dominated materials as $Ge_2Sb_2Te_5$ as compared to growth dominated alloys as $Ge_{12}Sb_{88}$. Therefore the values of $\alpha^3 \beta$ in table 1 explain the different nucleation behaviour of GeSbTe-based and AgIn-doped Sb_2Te on an atomistic base. While these values mostly describe the interfacial energy between the under-cooled liquid and the stable (hexagonal) phase it is still reasonable to assume, that both phases are fairly comparable to the amorphous and the rock-salt-phase, respectively. Hence these values also provide valuable insight into the reason for the different behaviour encountered upon crystallization of phase change films and are well in line with the growth-dominated re-crystallization mechanism for Sb-rich alloys stated above.

Table 1. Lower limit for the combined interfacial energy and entropy of fusion $\alpha^3 \beta$. Materials with higher values of this combined quantity are slow in nucleation because of the large energy costs of the interface between crystal and liquid [4].

	$Ge_{12}Sb_{88}$	AgIn-Sb_2Te	$Ge_4Sb_1Te_5$	$Ge_2Sb_2Te_5$
$\alpha^3 \cdot \beta$	0.024	0.017	0.016	0.008

4. Conclusions

A large number of chalcogenides crystallize in tetrahedral chalcopyrite or octahedral cubic-arrangements that can be understood in terms of their average valence electron number N_{sp}, which in turn is controlled by their stoichiometry. Although a detailed understanding of the origin of the optical contrast between the crystalline and amorphous phases cannot be established without a model for the amorphous phase, the tetrahedral arrangements tend to lower density and optical contrast and are thus in general not suitable for optical storage. For the Ge-containing alloys that crystallize in octahedral coordination we suggest a spinel-like short-range order for the amorphous phase with the Ge-atoms in fourfold coordination that explains the pronounced difference in the opto-electronic properties. A similar understanding of the kinetics still suffers from the lack of experiments with high spatial and time resolution. Future work should focus on kinetics to establish a similar understanding of the influence of stoichiometry in this field. From the structural point of view, other classes of phase change materials without Ge e.g. are the next promising field to be investigated in their amorphous phase.

References

[1] S. Ovshinsky: Phys. Rev. Lett. **21**, 1453 (1968).
[2] G.-F. Zhou, Mat. Sci. and Eng. **A 304-306**, 73-80 (2001).
[3] J. Kalb, F. Spaepen, M. Wuttig, Appl. Phys. Lett. **84**, 5240 (2004).
[4] J. Kalb, C. Wen, F. Spaepen. H. Dieker, M. Wuttig, J. Appl. Phys. **98**, 54910 (2005).
[5] R. Detemple, D. Wamwangi, M. Wuttig, G. Bihlmayer, Appl. Phys. Lett. **83**, 2572 (2003)
[6] M. Luo, M. Wuttig, Advanced Materials 16, 439 (2004).
[7] V. P. Zhuze, V. M. Sergeeva, E. L. Shtrum, Sov. Phys. **3**, 1925 (1958)
[8] H. Dieker, Diploma-Thesis, RWTH-Aachen Germany (2002).
[9] A. Kolobov, P. Fons, A. Frenkel, A. Ankudinov, J. Tominaga, T. Uruga, Nature Materials **3**, 703 (2004).
[10] C. E. Bouldin, R. A. Forman, M. I. Bell, Phys. Rev. B **35,** 1429 (1987).
[11] M. C. Ridgway, C. J. Glover, G. J. Foran, K. M. Yu, J. Appl. Phys. **83**, 4614 (1998).
[12] W. Welnic, A. Pamungkas, R. Detemple, C. Steimer, S. Blügel, M. Wuttig, Nature Materials **5**, 56 (2006).
[13] J. Kalb, PhD Thesis, RWTH-Aachen, Germany (2006) and to be published.

*Corresponding author: steimer@physik.rwth-aachen.de